Sahoo, H., et al., 2020, Predictable patterns in stacking and distribution of channelized fluvial sand bodies linked to channel mobility and avulsion processes: Geology, v. 48, https://doi.org/10.1130/G47236.1

Supplemental Material

Predictable patterns in stacking and distribution of channelized fluvial sand bodies linked to channel mobility and avulsion processes

Hiranya Sahoo, M. Royhan Gani, Nahid D. Gani, Gary J. Hampson, John A. Howell, Joep E.A. Storms, Allard W. Martinius, and Simon J. Buckley

1. Three-dimensional (3-D) Mapping of Channelized Sand Bodies from Lidar Data

For 3-D sand-body mapping and width correction, step-by-step procedures have been detailed in Sahoo and Gani (2015). Here we present the salient features of those steps and justifications for them. The nearly vertical, sparsely vegetated exposures of cliff faces in the study area and minimal structural distortion of strata provide a clear contrast between sandstones and mudstones (e.g., Fig. S1).

Figure S1. Example of cliff-face exposure in the study area.

Acquisition and processing procedures of the lidar data were detailed in Rittersbacher et al. (2013). Data were collected perpendicular to the outcrop faces, which ensured minimum parallax error in capturing the preserved dimensions of the sedimentologic elements exposed in the outcrop faces. The high resolution (~10 cm) of the lidar data set (Fig. 2D) was advantageous in distinguishing between sandstones and mudstones. As the 3-D lidar model is fully georeferenced, it allowed both the vertical and lateral dimensions of individual channelized sand bodies (henceforth "sand bodies") to be constrained, in addition to tracing their continuity from one cliff-face to the next with precision. The resulting virtual outcrop model has an areal extent of ~5 km x 5 km and thickness of ~300 m.

1.1. Distinction between Single-Story and Multilateral Sand Bodies

In our study, two fundamental types of sand bodies are identified: 1) a single-story sand body comprises a single bar-macroform combined with a laterally adjacent channel-fill deposit, and is characterized by a single basal surface of erosion (e.g., Potter, 1967); and 2) a multilateral sand body comprises multiple channel-story sand bodies that are laterally amalgamated at the same stratigraphic level, resulting in a composite basal surface of erosion (e.g., Potter, 1967; Gibling, 2006). The distinction between single-story and multilateral sand bodies is made using observations of stratal geometries in lidar (e.g., Figs. S2 and S3) and photographic data (Figs. 3C-3E; Fig. S10), supplemented by measured sections and paleocurrent data from accessible outcrops in the study area and in nearby locations in the Wasatch Plateau outcrop belts (Hampson et al., 2013; Sahoo and Gani, 2016; Sahoo et al., 2016). Single-story sand bodies and stories within multilateral sand bodies have many similar characteristics: (1) their bases are

Figure S2. Multilateral sand body mapped in the lidar data (upper diagram: uninterpreted; lower diagram: interpreted). Two single-story sand bodies are laterally amalgamated at the same stratigraphic level. Red: channel-story base, blue: channel-story top.

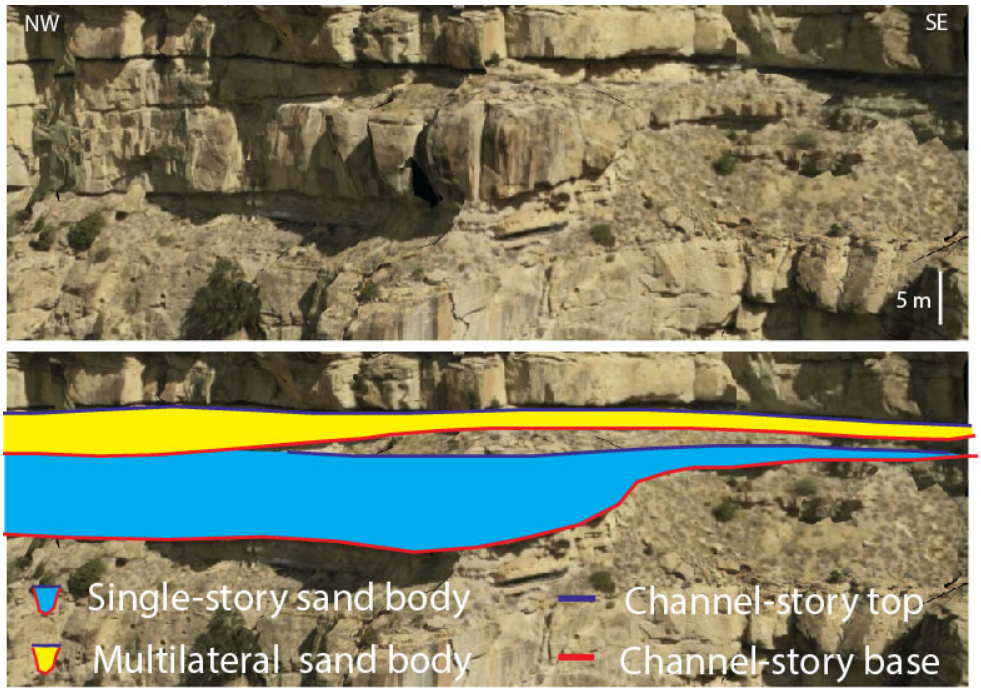

Figure S3. Lidar data (upper diagram: uninterpreted; lower diagram: interpreted) illustrating a reoccupational stacking pattern in which a single-story sand body is overlain by a multilateral sand body. For its photographic data, see Fig. 3C. Floodplain deposits are intercalated between underlying single-story sand body and overlying multilateral sand body.

marked by laterally discontinuous mudclast lags; (2) they comprise medium-grained sandstones that grade upwards into fine-grained sandstones; (3) lateral-accretion sets at story margins are common; (4) dune-scale cross-bedding is the predominant sedimentary structure; and (5) siltstone and mudstone beds are absent (Hampson et al., 2013; Flood and Hampson, 2014; Sahoo and Gani, 2016; Sahoo et al., 2016). In the 3-D lidar data set (e.g., Fig. S4; aided by outcrop photos like Fig. S1), we mapped each channel-story individually by tracing their top-bounding surface (blue color) and basal-erosion surface (pink color) (Figs. S5 and S6).

Tracking the continuity of each single-story sand body, either isolated laterally or forming part of a multilateral sand body, was performed across cliff faces using a combination of observational constraints: (1) the top of the shallow-marine Star Point Formation, which underlies the Blackhawk Formation (Fig. S4), is exposed throughout the study area and was used as a datum surface from which the sand body altitude (i.e., *z* value of the sand-body top, after adjusting for the minor structural dip of ~5^0 towards the west) was monitored (Fig. S5); (2) the thickness of each sand body was assumed to remain similar along its axis, in depositional-dip orientation, over the extent of the study area (~5 km); and (3) we also used regionally extensive coal zones within the study area (e.g., Axel Anderson, Blind Canyon, and Bear Canyon; Fig. S4) as reference surfaces to check the stratigraphic positions of the sand bodies.

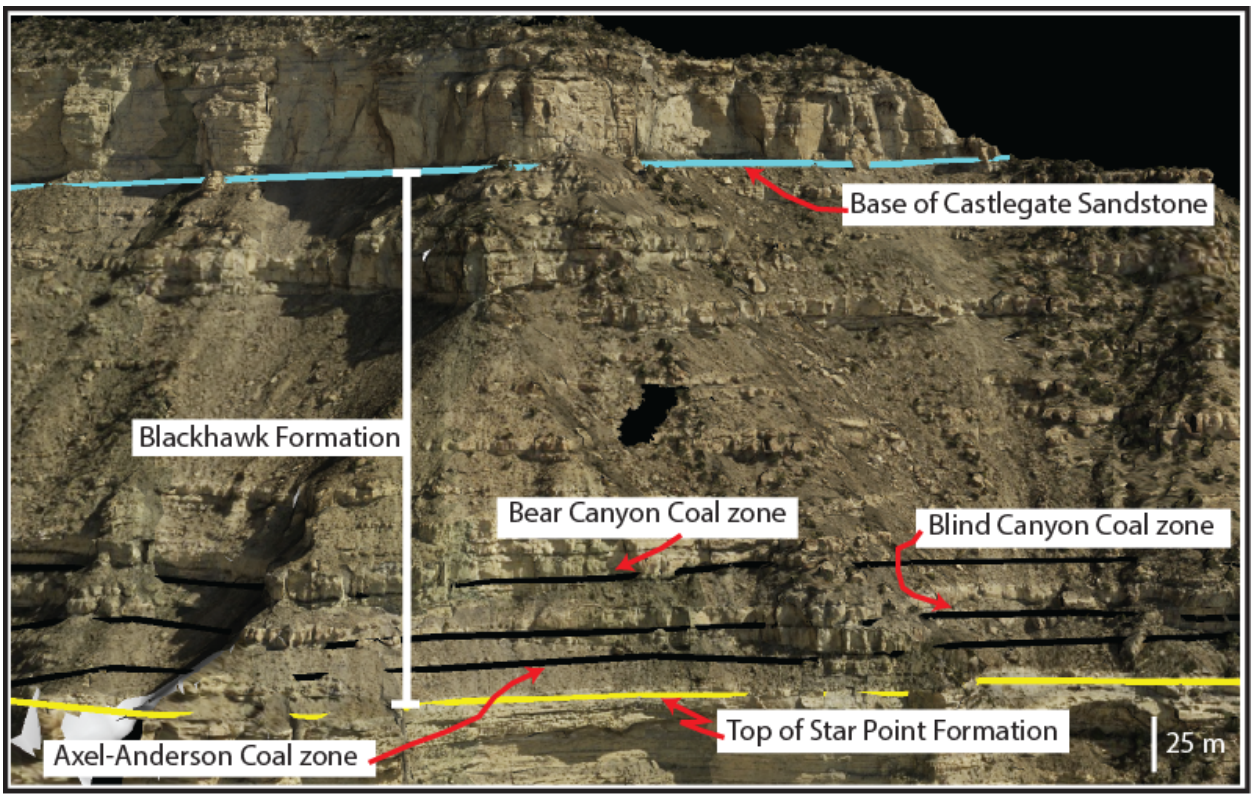

Figure S4. Lidar data showing the Star Point Formation, Blackhawk Formation, and Castlegate Sandstone, along with three regionally extensive, well-defined coal zones in the Blackhawk Formation. The data are from cliff face 6 shown in Figs. 2B-2D.

1.2. Estimation of True Sand-body Width

After mapping all sand bodies exposed at outcrop (Fig. S6), we undertook their width correction. Sand bodies produced by channel migration are oriented along the mean flow direction, instead of along the localized, variable azimuth of the paleochannel axis, such that abundant paleoflow data were needed to delineate the correct sand body orientations. We collected paleoflow data from lateral-accretion surfaces, dune and ripple cross-stratification in the Blackhawk Formation (n = 236) from cliff faces 1, 2 and 6 (Fig. 2). These data were grouped by stratigraphic position (lower, middle, and upper Blackhawk Formation; Fig. S7). We

calculated the vector mean of paleocurrents for the entire data set (N050), as well as separately for the lower (N047), middle (N057), and upper (N045) Blackhawk Formation (Fig. S7).

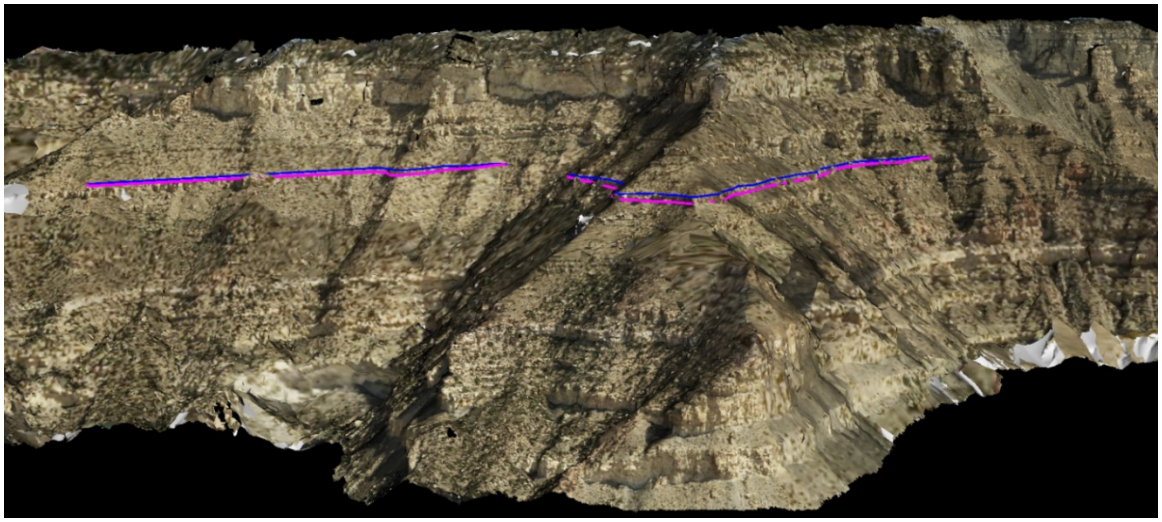

Figure S5. Examples of mapped sand-body base (pink color) and top (blue color) across the 3-D lidar data set. Outcrop is 483 m high. The data are from cliff faces 3 and 4 shown in Figs. 2B-2D.

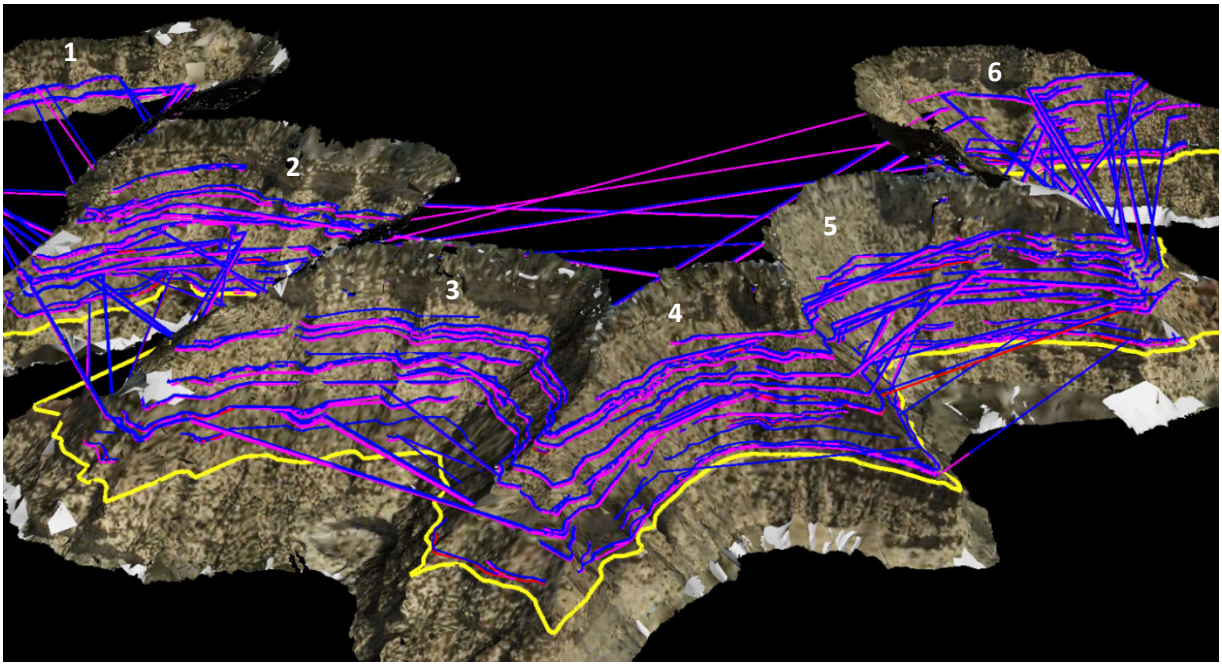

Figure S6. 3-D perspective view of tops and bases of mapped sand bodies in the lidar data set. Numbers denote cliff faces 1-6 shown in Figs. 2B-2D.

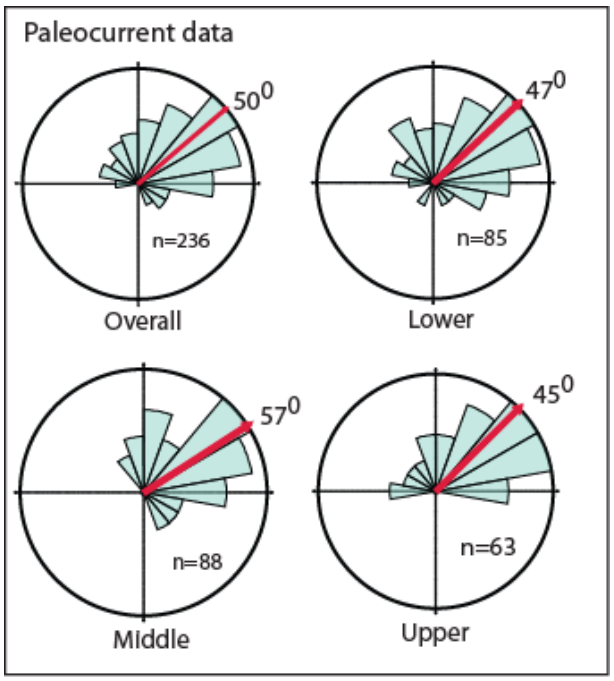

Figure S7. Paleocurrent data from the Blackhawk Formation in the study area.

As the overall vector mean (N050) shows consistency with the vector mean values of the lower, middle, and upper Blackhawk Formation, we considered it to be a representative paleocurrent value for the entire data set. Moreover, this vector mean value (N050) is also broadly consistent with the regional paleoflow direction of the Blackhawk Formation (Hampson et al., 2012; Rittersbacher et al., 2013). We carried out the width correction of mapped sand bodies perpendicular to the paleoflow vector mean in the ArcMap platform (Fig. S8). The procedure of sand body width-correction was performed on a projection plane aligned perpendicular to the mean paleoflow direction (cf., Fabuel-Perez et al., 2009; Rittersbacher et al., 2013).

As the depositional-dip extent of the study area is only ~5 km, it is reasonable to assume sand bodies to be linear and of uniform width at this scale (cf., Holbrook et al., 2006). With this assumption, all single-story and multilateral sand bodies with their corrected widths (Table S1)

were projected onto a plane perpendicular to the mean paleoflow direction (Line S-T in Fig. 2C), in order to investigate the stratigraphic organization of these sand bodies.

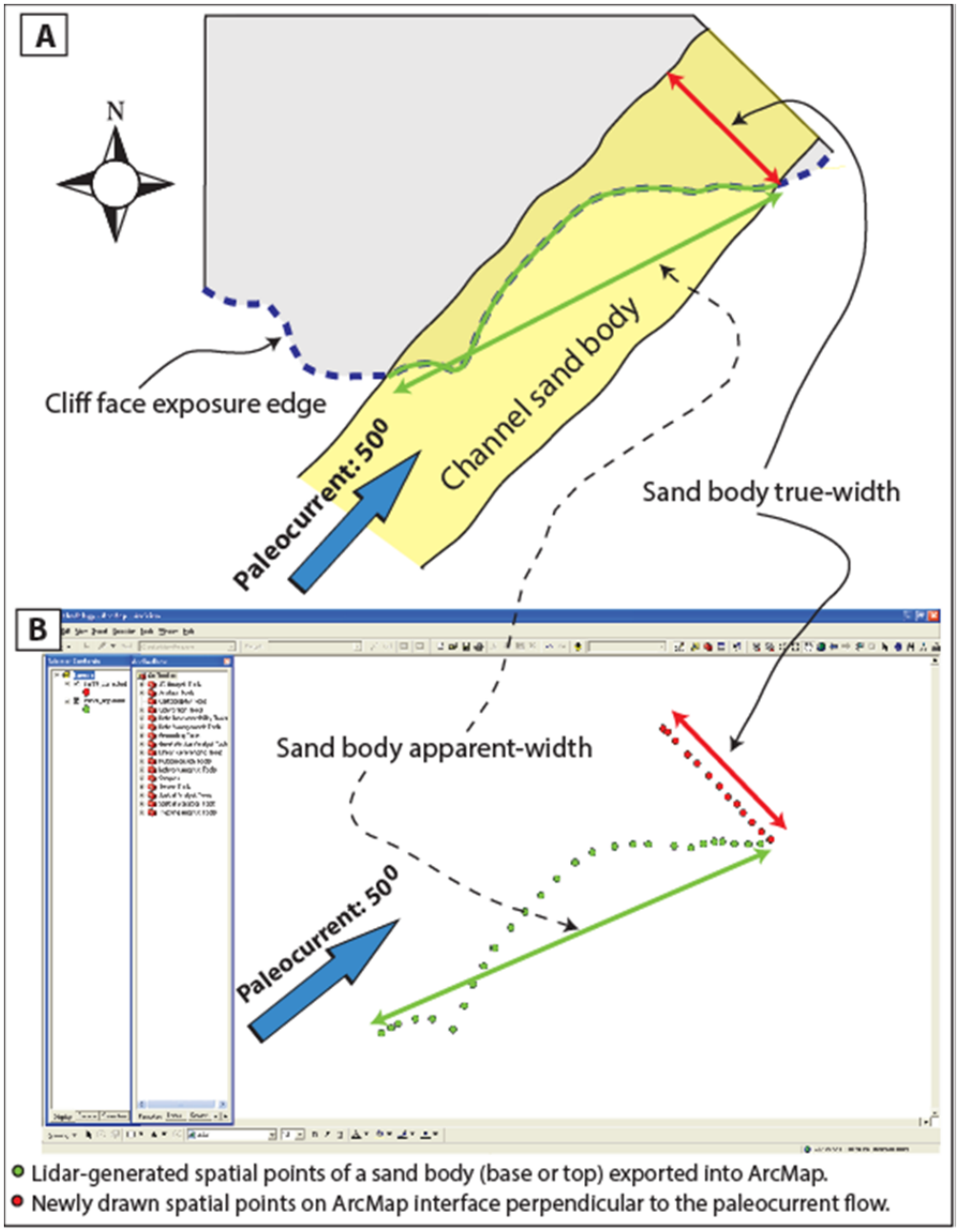

Figure S8. Width correction of sand body. A) The cliff face exposes the apparent width of a sand body instead of its true width. B) Points denoting the spatial position of the sand body in the lidar-generated outcrop model were imported to ArcGIS (green points). A new set of spatial points (red points) was drawn perpendicular to the mean paleocurrent direction in order to calculate the true sand-body width.

Table S1. Width-corrected dimensions of single-story and multilateral sand bodies that were mapped in the study area. Mean values are listed in bold at the end of each column.

Single-story			Multilateral		
Width (m)	Thickness (m)	Aspect ratio	Width (m)	Thickness (m)	Aspect ratio
80	4	20	270	5	54
50	3	17	704	6	117
90	3	30	795	6	133
91	21	4	204	3	68
57	4	14	273	6	46
130	10	13	682	4	171
136	5	27	295	4	74
91	5	18	886	5	177
45	4	11	932	5	186
95	7	14	280	5	56
114	8	14	375	4	94
114	15	8	523	5	105
73	7	10	295	3	98
68	5	14	841	3	280
67	4	17	227	4	57
68	4	17	454	3	151
91	5	18	909	5	182
75	25	3	227	4	57
114	6	19	432	5	86
70	5	14	1000	4	250
72	6	12	909	4	227
71	5	14	227	4	57
88	7	13	250	4	63
75	5	15	591	6	99
94	7	13	1204	6	201
102	8	13	772	6	129
91	13	7	273	4	68
114	6	19	886	5	177
91	15	6	318	4	80
115	6	19	841	5	168
92	6	15	386	5	77
113	23	5	295	4	74
112	5	22	863	5	173
227	5	45	273	5	55
93	**8**	**15**	795	5	159
			704	7	101
			1000	5	200
			1136	5	227
			523	6	87
			1181	6	197
			477	5	95
			1181	7	169
			1159	4	290
			772	4	193
			795	9	88
			500	6	83
			545	5	109
			627	**5**	**129**

2. Ground-truthing of Lidar Data

Both fine-grained floodplain deposits and sand bodies have been characterized at outcrop using observations acquired by climbing cliff faces 1, 2 and 6 (Figs. 2B and 2C). Field documentation included descriptions of lithology, grain size, sedimentary structures, and paleoflow data. Latitude, longitude, and elevation values for these data were collected using a handheld Tremble GPS of sub-meter accuracy. Dune-scale cross-set thickness data were grouped for single-story and multilateral sand bodies. A subsurface core (EM-137C) that is centrally located in the study area (Fig. 2C) was logged in detail (Fig. S9). Without core, detailed characterization of floodplain deposits is challenging from outcrop data alone due to vegetation and scree cover. Well-developed coal seams are developed preferentially in the lower part of the Blackhawk Formation (Fig. 3A; Fig. S9), implying that a highly vegetated floodplain was developed at certain times, generally coincident with regional shoreline transgression (Hampson et al., 2012). Other types of floodplain deposit lack a pattern in their vertical distribution (Fig. S9), as noted in other parts of the Wasatch Plateau outcrop belt (Flood and Hampson, 2014). Single-story and multilateral sand bodies were interpreted in the field based on their internal architecture (e.g., Figs. 3C-3E; Fig. S10C).

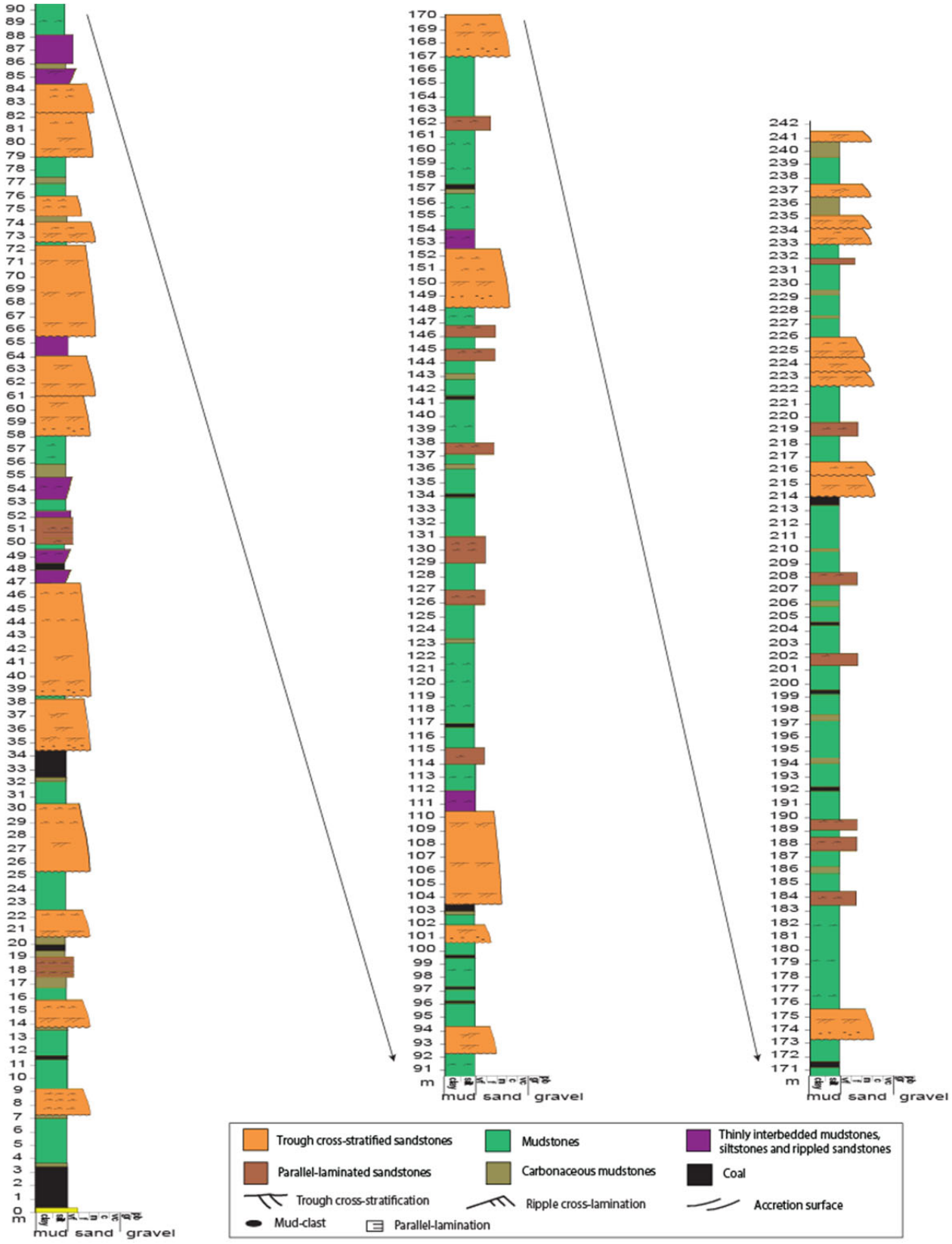

130

131 Figure S9. Detailed sedimentological description of the EM-137C core (located in Figs. 2B and 2C).

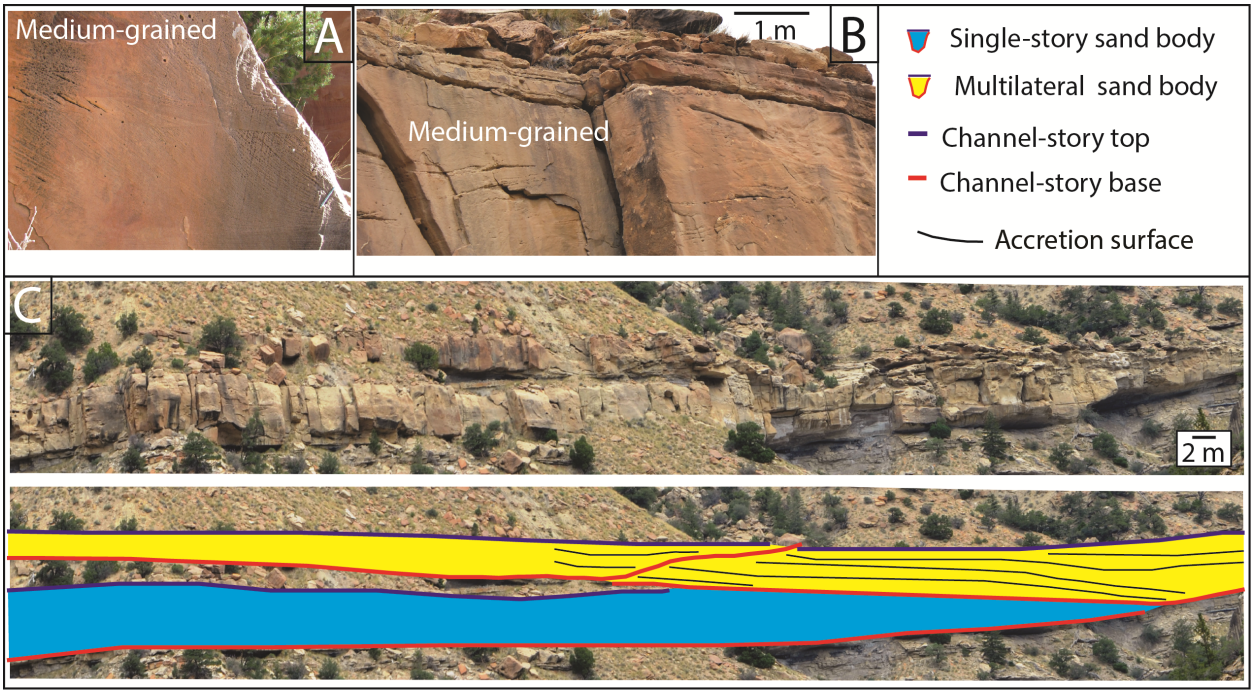

Figure S10. Outcrop characterization of sand bodies and their stratigraphic stacking pattern. See Figure 3A for the stratigraphic positions of the illustrated sand bodies. A) Part of multilateral sand body (medium-grained) containing dune cross-stratification (Fig. 3A). B) Single-story sand body (medium-grained) containing dune cross-stratification (Fig. 3A). C) Single-story sand body overlain by multilateral sand body in a sand-body cluster (Fig. 3A). Floodplain deposits are intercalated between underlying single-story sand body and overlying multilateral sand body.

3. Paleohydraulic Analysis to Estimate Paleochannel Parameters

The studied outcrops contain only one fully preserved paleochannel (Fig. S11B), which provides little constraint on paleochannel dimensions. Therefore, we estimated paleochannel depth and width using a combination of outcrop data (e.g., dune-scale cross-set thickness, dip extent of lateral-accretion bed, and bar height) and well-established paleohydraulic relationships (cf., Hampson et al., 2013 and references therein; Gani and Gani, 2011 and references therein). Such paleohydraulic analysis of outcrop data has become a useful means of

147 deriving paleochannel parameters (e.g., Hampson et al., 2013; Holbrook and Wanas, 2014;
148 Bhattacharya et al., 2016).
149
150 **3.1. Flow-depth Estimation**
151 From compiled dune-scale cross-set thickness data, the mean cross-set thickness (S_m) and
152 standard deviation (S_{sd}) were calculated. When S_m/S_{sd} is ~0.88, average dune height (h_m) can be
153 estimated as (Le Clair and Bridge, 2001; Bridge and Tye, 2000):
154 $$h_m = 5.3\,\beta + 0.001\beta^2 \qquad (1)$$
155 $$\beta \approx S_m / 1.8 \qquad (2)$$
156 Flow-depth scales to 6-10 times the average dune height. Accordingly, the bankfull flow depth
157 of paleochannels was estimated.
158 Additionally, the bankfull flow depth of paleochannels was estimated from the thickness
159 of a fully preserved bar sand-body (T_h) using the equation:
160 $$\text{Bankfull flow depth} = T_h/0.9 \qquad (3)$$
161 Using the above two approaches, we have compiled estimates of bankfull flow depth for the
162 paleochannels forming single-story and multilateral sand bodies (Fig. 4C).
163
164 **3.2. Channel-width Estimation**
165 Bankfull channel width can be estimated as (Bridge and Mackey, 1993; Bridge and Tye, 2000):
166 $$W = 8.88(d_m)^{1.82} \qquad (4)$$
167 Where d_m is the mean bankfull channel depth. Using Equation 4, we estimated bankfull width
168 values of paleorivers forming single-story and multilateral sand bodies.

Paleochannel-width values derived from paleohydraulic analysis of sand bodies at different stratigraphic positions have a narrow range (100-160 m). The resulting mean paleochannel width (115 m) is consistent not only with other mean values estimated for paleochannels in nearby exposures of the Blackhawk Formation (Rittersbacher et al., 2014; Hampson et al, 2013) but also with the directly measured value of 100 m of the preserved abandoned-channel fill in the study data set (Fig. S11). Given this similarity, we estimated a final mean value for paleochannel width of 106 m (Fig. S11A).

Paleochannel parameters

A

i. From paleohydraulics estimation	Channel depth mean (m)	Channel width mean (m)
This study	Fig. 4C of main paper	115
Hampson et al. (2013)	7	95
Rittersbacher et al. (2014)		116
ii. From mud-filled abandoned paleochannel (this study; Fig. S11B)	8	100
Final mean value (FMV)		106

B

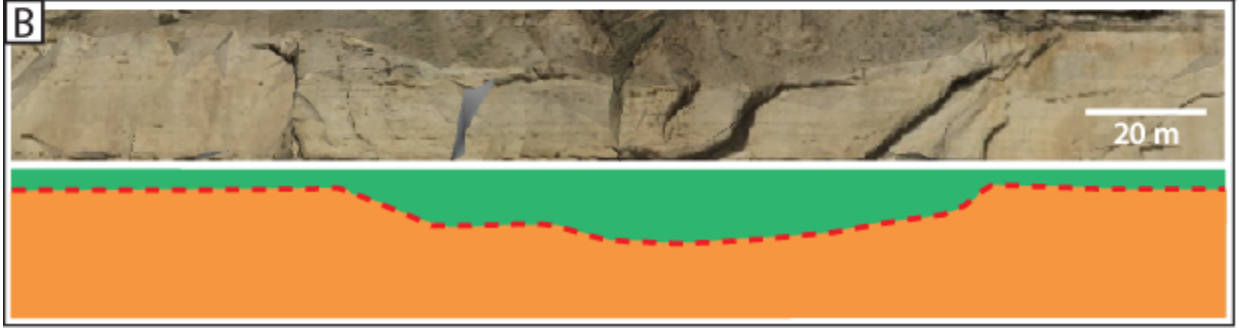

Figure S11. Derivation of paleochannel dimensions from paleohydraulic analysis in this study and previous studies (A), and from direct measurement of abandoned-channel (B).

4. Channel-mobility Index (*M*)

Channel mobility implies a rate, which has been quantitatively assessed in modern systems (e.g., Jerolmack and Mohrig, 2007; Blum et al., 2013). However, constraining rates from analysis of ancient strata is almost impossible, given the sparse sampling and low resolution of available age data, as has been pointed out by recent studies (e.g., Jobe et al., 2016). Jobe et al. (2016) instead used channel geomorphic expression (i.e., abandoned channel fills), paleohydraulic estimates, and sand-body dimensions to conduct mobility analysis in ancient strata (e.g., derivation of their 'stratigraphic mobility number'). Here we have taken a similar approach to channel mobility analysis in our data set, using channel geomorphic expression (i.e., abandoned channel fills; e.g., Fig. S11), paleohydraulic estimates (Section 3) and sand-body dimensions (Table S1).

We define channel mobility as the degree of lateral channel migration on the floodplain prior to avulsion (cf. Gibling, 2006; Jerolmack and Mohrig, 2007). To analyze this parameter, we develop a dimensionless channel-mobility index, *M*, where:

$$M = \text{width of sand body} / \text{width of paleochannel}$$

Here, 'width of sand body' denotes the near-true width calculated for each sand body (methodology described in Section 1.2, and values in Table S1), and 'width of paleochannel' is the final estimate of mean paleochannel width (106 m) that we derived from paleohydraulic analysis (methodology described in Section 3; Fig. S11). Since paleohydraulic analysis is used to estimate mean 'width of paleochannel', values of *M* are indicative, and some physically unrealistic values <1 are calculated. *M* provides a quantitative proxy of the extent to which a formative channel was laterally mobile with respect to its width, in depositing a sand body.

Frequency distributions of *M* values have been calculated for single-story and multilateral sand bodies in the study data set (Figs. 4D and 4E).

We also performed a sensitivity test to evaluate how estimation of *M* varies when using final mean value (106 m) and extreme values of channel width (lowest 100 m, and highest 160 m). *M* estimations for these three cases of channel width show only small variability (STD = 0.1-2).

5. Depocenter Shift from Multilateral Sand Body to Single-story Sand Body

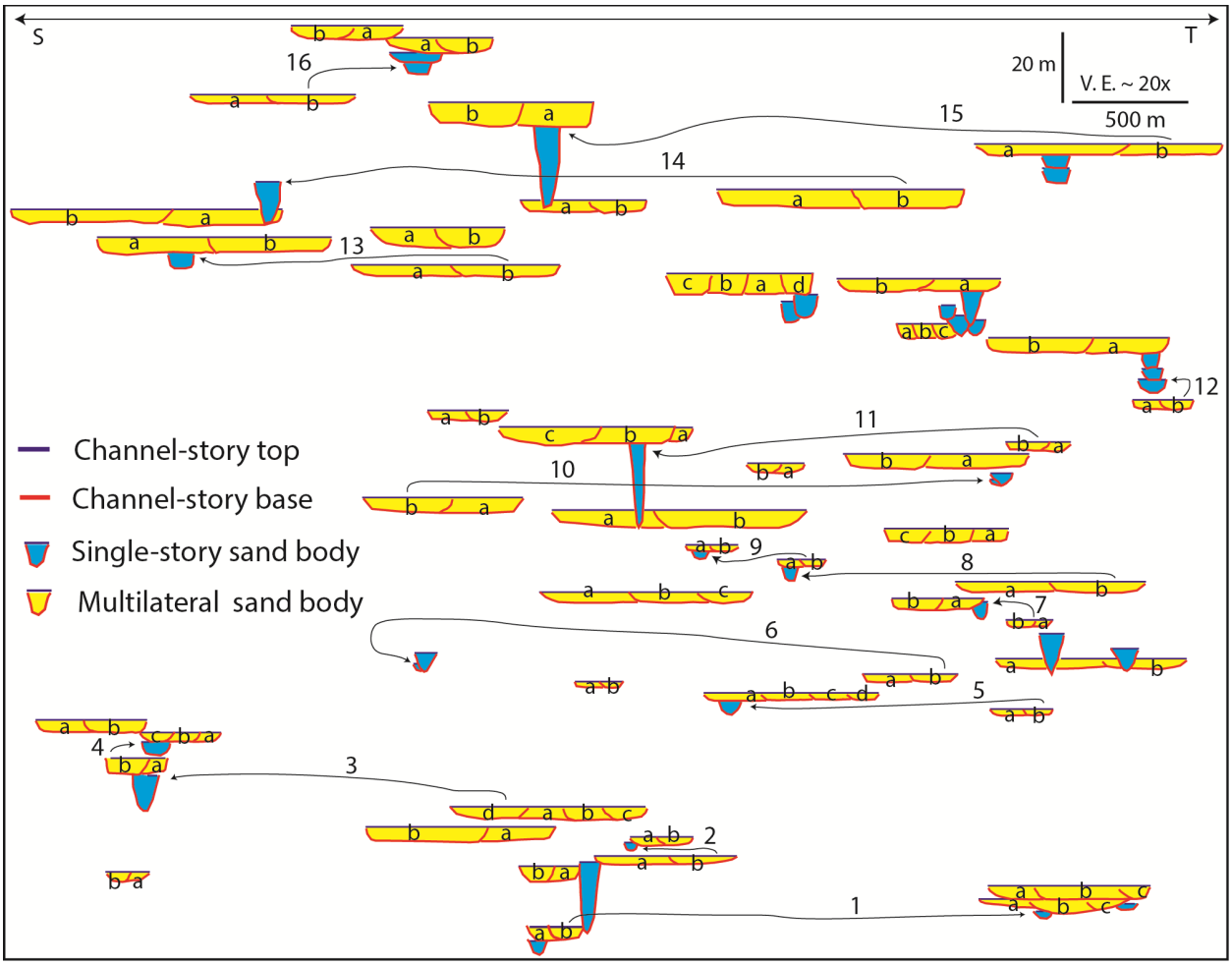

Figure S12. Examples (n = 16) on study data set, in which depocenter shifts stratigraphically from a multilateral (preceding sand body) to single-story (succeeding sand body), assuming that sand-body relative age corresponds to height above the datum at the base of the transect (i.e., top of Star Point Formation; Fig. S4). These examples illustrate an inferred compensational stacking pattern of sand bodies, since the preceding multilateral sand bodies are not vertically stacked (no channel reoccupation).

References

Bhattacharya, J.P., Copeland, P., Lawton, T. F., and Holbrook, J., 2016, Estimation of source area, river paleo-discharge, paleoslope, and sediment budgets of linked deep-time depositional systems and implications for hydrocarbon potential: Earth-Science Reviews, v. 153, p. 77-110.

Blum, M., Martin J., Milliken, K., and Garvin, M., 2013, Paleovalley systems: Insights from Quaternary analogs and experiments: Earth-Science Reviews, v. 116, p. 128–169.

Bridge, J. S., and Tye, R. S., 2000, Interpreting the dimensions of ancient channel bars, channels, and channel belts from wireline-logs and cores: American Association of Petroleum Geologists Bulletin, v. 84, no. 8, p. 1205-1228.

Bridge, J. S, and Mackey, S. D., 1993, A theoretical study of fluvial sandstone body dimensions, in S. S. Flint and I. D. Bryant, eds., The geological modeling of hydrocarbon reservoirs and outcrop analogues: International Association of Sedimentologists Special Publication No. 15, p. 3-20.

Fabuel-Perez, I., Hodgetts, D., and Redfern, J., 2009, A new approach for outcrop characterization and geostatistical analysis of a low-sinuosity fluvial-dominated succession using digital outcrop models: Upper Triassic Oukaimeden Sandstone Formation, central High Atlas, Morocco: AAPG Bulletin, v. 93, p. 795-827.

Flood, Y.S., and Hampson, G.J., 2014, Facies and architectural analysis to interpret avulsion style and variability: Upper Cretaceous Blackhawk Formation, Wasatch Plateau, central Utah, USA: Journal of Sedimentary Research, v. 84, p 743–762.

Gani, M. R., and Gani, N. D., 2011, River-margin habitat of Ardipithecus ramidus at Aramis, Ethiopia 4.4 million years ago: Nature Communications 2, 602. doi:10.1038/ncomms1610.

Gibling, M.R., 2006, Width and thickness of fluvial channel bodies and valley fills in the geological record: a literature compilation and classification: Journal of Sedimentary Research, v. 76, p. 731–770.

Hampson, G. J., Jewell, T. O., Irfan, N., Gani, M. R., and Bracken, B., 2013, Modest change in fluvial style with varying accommodation in regressive alluvial-to-coastal-plain wedge: upper cretaceous Blackhawk Formation, Wasatch Plateau, central Utah, U.S.A.: Journal of Sedimentary Research, v. 83, p. 145-169.

Hampson, G. J., Gani, M. R., Sahoo, H., Rittersbacher, A., Irfan, N., Ranson, A., Jewell, T. O., Gani, N. D. S., Howell, J. A., Buckley, S. J., and Bracken, B., 2012, Controls on large-scale patterns of fluvial sandbody distribution in alluvial to coastal plain strata: Upper Cretaceous

279 Blackhawk Formation, Wasatch Plateau, Central Utah, USA: Sedimentology, v. 59, p. 2226-
280 2258.
281
282 Holbrook, J., and Wanas, H., 2014, A Fulcrum Approach To Assessing Source-To-Sink Mass
283 Balance Using Channel Paleohydrologic Paramaters Derivable From Common Fluvial Data
284 Sets With An Example From The Cretaceous of Egypt: Journal of Sedimentary Research, v.
285 84, p. 349–372.
286
287 Holbrook, J., Scott, R.W., and Oboh-ikuenobe, F.E., 2006, Base-level buffers and buttresses: a
288 model for upstream versus downstream control on fluvial geometry and architecture within
289 sequences: Journal of Sedimentary Research, v. 76, p. 162–174.
290
291 Jerolmack, D.J., and Mohrig, D., 2007, Conditions for branching of rivers: Geology, v. 35, p. 463-
292 466.
293
294 Jobe, Z.R., Howes, N. C., and Auchter, N. C., 2016, Comparing submarine and fluvial channel
295 kinematics: Implications for stratigraphic architecture: Geology, v. 44, p. 931-934.
296
297 Le Clair, S.F., and Bridge, J.S., 2001, Quantitative interpretation of sedimentary structures
298 formed by river dunes: Journal of Sedimentary Research, v. 71, p. 713-716.
299
300 Potter, P.E., 1967, Sand bodies and sedimentary environments: a review: American Association
301 of Petroleum Geologists Bulletin, v. 51, p. 337–365.
302
303 Rittersbacher, A., Buckley, S.J., Howell, J.A., Hampson, G.J., and Vallet, J., 2013, Helicopter-
304 based laser scanning: a method for quantitative analysis of large-scale sedimentary
305 architecture, in Martinius, A.W., Howell, J. A., and Good, T., eds., Sediment-body Geometry
306 and heterogeneity: Analogue studies for modelling the subsurface: Geological Society of
307 London, Special Publication 387, published online first, unpaginated.
308
309 Sahoo, H., and Gani, N.D., 2015, Creating three-dimensional channel-bodies in Lidar-integrated
310 outcrop characterization: A new approach for improved stratigraphic analysis: Geosphere,
311 v. 11, p. 777-785, doi:10.1130/GES01075.1.
312
313 Sahoo, H., and Gani, M.R., 2016, Autogenic Modulation of Fluvial Channel Fills in Allogenically
314 Formed Incised Valleys: Cretaceous Blackhawk Formation, USA, *in* Budd, D., et al., eds.,
315 Autogenic Dynamics and Self-Organization in Sedimentary Systems: Society for Sedimentary
316 Geology (SEPM) Special Publication 106, p. 163-175.
317 https://doi.org/10.2110/sepmsp.106.08.
318
319 Sahoo, H., Gani, M.R., Hampson, G.J., Gani, N.D., and Ranson, A., 2016, Facies-to sandbody-
320 scale heterogeneity in a tight-gas fluvial reservoir analog: Blackhawk Formation, Wasatch
321 Plateau, Utah, USA: Marine and Petroleum Geology, v. 78, p. 48-69.